International Journal on Advanced Science Engineering Information Technology

Vol.10 (2020) No. 3
ISSN: 2088-5334

A Staggered Method for Simulating Shallow Water Flows along Channels with Irregular Geometry and Friction

Bambang Agus Sulistyono[a,b,1], Leo Hari Wiryanto[a,2], Sudi Mungkasi[c]

[a] *Department of Mathematics, Faculty of Mathematics and Natural Sciences, Institut Teknologi Bandung, Bandung, Indonesia*
E-mail: [1]bb7agus1@gmail.com, [2]leo@math.itb.ac.id

[b] *Department of Mathematics Education, Universitas Nusantara PGRI Kediri, Kediri, Indonesia*

[c] *Department of Mathematics, Faculty of Science and Technology, Universitas Sanata Dharma, Yogyakarta, Indonesia*
E-mail: sudi@usd.ac.id

***Abstract*— We consider the shallow water equations along channels with non-uniform rectangular cross sections with source terms due to bottom topography, channel width, and friction factor. The system of equations consist of the mass and momentum conservation equations. We have two main goals in this paper. The first is to develop a numerical method for solving the model of shallow water equations involving those source terms. The second is to investigate effects of friction in water flows governed by the model. We limit our research to the flows of one-dimensional problems. The friction uses the Manning's formula. The mathematical model is solved numerically using a finite volume numerical method on staggered grids. We propose the use of this method, because the computation is cheap due to that no Riemann solver is needed in the flux calculation. Along with a detailed description of the scheme, in this paper, we show a strategy to include the discretization of the friction term in the staggered-grid finite volume method. Simulation results indicate that our strategy is successful in solving the problems. Furthermore, an obvious effect of friction is that it slows down water flows. We obtain that great friction values lead to slow motion of water, and at the same time, large water depth. Small friction values result in fast motion of water and small water depth.**

***Keywords*— friction term; irregular channel width; irregular geometry; irregular topography; shallow water equations.**

I. INTRODUCTION

Water flow appears in everyday life. Flows can be in either a closed channel or free surface channel. An example of closed-channel flow is pipe flow. Examples of free surface flows are those in rivers, lakes, seas, and reservoirs. They can be in the forms of floods, tsunamis, and others. This paper focuses on free surface water flows.

A large number of studies have been done by researchers relating to water flows. One of the most famous results is the Saint-Venant model [1]. This model can be applied to simulate shallow water waves or flows. The original Saint-Venant model has been developed by a number of researchers. The model has currently a number of improvements and variations. Some improvements and variations involve topography, some other involve irregular channel width, and the rest involve friction factor [2], [3], [4], [5], [6]. Based on its form, the Saint-Venant model is a partial differential equation system. Based on physics, the form of the equation can be either conservative or non-conservative [7], [8], [9].

One of the Saint-Venant model variations is the system of one-dimensional shallow water equations. This system or model can be used for various types of free surface flows with irregular topography and irregular channel width. Mungkasi *et al.* [8] solved this model using a staggered-grid finite volume method. This method has a very simple flux calculation, which leads to cheap computation, as developed by Stelling and Duinmeijer [10]. However, Mungkasi *et al.* [8] did not involve any friction in their shallow water model. The work of Mungkasi *et al.* [8] is extended in the present paper by including the friction factor in our water flow problems.

In this paper, we have two goals. First, we develop a numerical scheme of the finite volume method on staggered grids to approximate solutions to the shallow water equations with source terms due to bottom topography, channel width, and Manning friction. Second, we investigate the influences or effects of the friction to water flows.

A finite volume method is chosen, as our problems admit continuous and discontinuous solutions. Some research of finite volume methods has been reported in the literature, such as [11], [12]. Based on the positions of grids for evaluation of the unknown variables, finite volume methods are categorized into two types, namely, the collocated and staggered methods. Some works on collocated-grid finite volume methods are [13], [14], [15], [16]. Some works on staggered-grid finite volume methods are [8], [10]. An application of these works is, for example, in simulation of the flood routing problem [17], [18], [19], [20].

The rest of this paper follows. Section II recalls the mathematical model and writes our proposed numerical method. Simulation results are presented and discussed in section III. Conclusion is given in section IV.

II. Material and Method

A. Mathematical Model

We consider one-dimensional shallow water flows with irregular bottom topography, irregular channel width, and friction. Schematic illustrations of this flow problem are shown in Fig.1 including the geometries of the transversal cross section, the longitudinal flow, and the flow space viewed from the top.

(a). Illustration of the transversal cross section

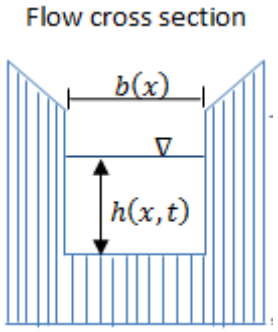

(b). Illustration of the longitudinal flow

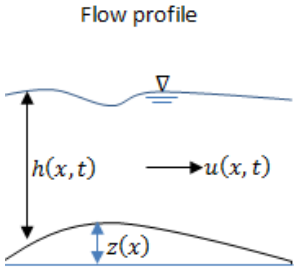

(c). Illustration of the flow space viewed from the top

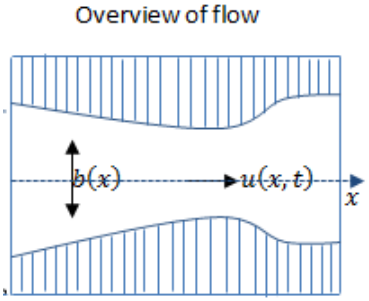

Fig.1. Schematics for shallow water flows along a channel with irregular topography and irregular width in three different points of view.

Water flows in open channels such as rivers and canals can be modeled by a partial differential equation system. This system can be expressed in the forms of mass conservation equation and momentum balance equation, respectively, as follows [3]:

$$A_t + Q_x = 0, \tag{1}$$

$$Q_t + \left(Q^2/A\right)_x + gAh_x + gA\left(S_f - S_0\right) = 0. \tag{2}$$

Here, h is the surface level of water in the channel, Q represents the discharge, A denotes the wet cross-sectional area of the flow, S_0 is the slope of bottom of the channel, S_f is the friction slope, g is the gravitational acceleration, x represents the longitudinal distance along the channel, and t is the time variable.

The friction slope S_f can be obtained from the Manning friction formula as:

$$S_f = \frac{n^2 Q|Q|}{A^2 R^{4/3}} \tag{3}$$

where n represents the Manning's friction coefficient and R is the hydraulic radius.

By substituting the following expressions, that is, $A = bh$, $Q = bhu$, and $S_0 = -z_x$, to (1) and (2), then we obtain:

$$(bh)_t + (bhu)_x = 0 \tag{4}$$

and

$$(bhu)_t + \left(bhu^2 + \tfrac{1}{2}gh^2 b\right)_x = -ghbz_x + \tfrac{1}{2}gh^2 b_x - gbhS_f \tag{5}$$

where $z = z(x)$ is the irregular bottom topography, $b = b(x)$ represents the irregular channel width, $u(x,t)$ denotes the velocity, and

$$S_f = \frac{(2h+b)}{bh} n^2 u|u|$$

is again the Manning friction formula. Further, (4) and (5) are rewritten as:

$$h_t + (hu)_x = -\frac{hub_x}{b} \tag{6}$$

and

$$(hu)_t + \left(hu^2 + \tfrac{1}{2}gh^2\right)_x = -\frac{hu^2 b_x}{b} - ghz_x - ghS_f. \tag{7}$$

In this paper, (6) and (7) are the mathematical model which shall be solved numerically using the method with staggered grids. The system of (6) and (7) is the shallow water equations in one dimension that model flows along channels with irregular rectangular cross section of channel width and irregular bottom topography involving friction.

B. Numerical Method

In this subsection, we continue the work of Mungkasi *et al.* [8] as well as Stelling and Duinmeijer [10] in developing the staggered-grid finite volume method, or the staggered method, in short. There was no variation of channel width in the work of Stelling and Duinmeijer [10] for one-dimensional problems. There was no friction in the model solved by Mungkasi *et al.* [8]. The problems in the present paper involve irregular topography, irregular channel width, and friction.

To discretize the governing equations, without loss of generality, in this subsection we consider (6) and (7) with the spatial domain $0 \le x \le L$ using the partition:

$$x_{1/2} = 0,\ \ldots,\ x_{i-1/2},\ x_i,\ x_{i+1/2},\ \ldots,\ x_{N+1/2} = L.$$

As we work on the numerical method with staggered-grids, values of depth h are approximated at full grid points x_i for $i = 1, \ldots, N$ and the values of velocity u are approximated at half grid points $x_{i+1/2}$ for $i = 0, 1, \ldots, N$. We consider (6) and (7) on different control volumes, as shown in Fig. 2. We calculate the depth h using the mass conservation (6) at the control volume $[x_{i-1/2}, x_{i+1/2}]$ and the velocity u using the momentum balance (7) at the control volume $[x_i, x_{i+1}]$.

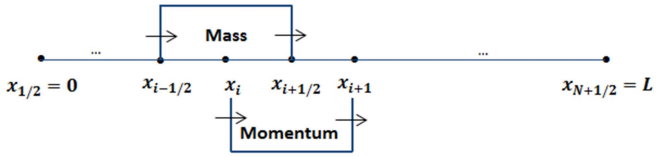

Fig. 2 A configuration of one-dimensional staggered grids, in which the full points are assigned for the mass conservation and the half points are assigned for the momentum balance.

We denote $h_i^k \approx h(x_i, t^k)$ and $u_{i+1/2}^k \approx u(x_{i+1/2}, t^k)$, where $x_i = x_{i-1} + \Delta x$ and $t^k = t^{k-1} + \Delta t$ for all involved integers i and k.

The spatial discretization of (6) and (7) are:

$$\frac{dh_i}{dt} = -\frac{q_{i+1/2}^k - q_{i-1/2}^k}{\Delta x} - \frac{h_i^k\, {}^*u_i^k \left(b_{i+1/2} - b_{i-1/2}\right)}{b_i \Delta x} \tag{8}$$

and

$$\begin{aligned} \frac{d\bar{h}_{i+1/2} u_{i+1/2}}{dt} &= -\frac{1}{2} g\left(h_{i+1}^{k+1}\right)^2 - \left(h_i^{k+1}\right)^2 \\ &- \frac{\bar{q}_{i+1}^{\,k}\, {}^*u_{i+1}^k - \bar{q}_i^{\,k}\, {}^*u_i^k}{\Delta x} - \frac{q_{i+1/2}^k u_{i+1/2}^k \left(b_{i+1} - b_i\right)}{b_{i+1/2} \Delta x} \\ &- g \bar{h}_{i+1/2}^{k+1} \frac{z_{i+1} - z_i}{\Delta x} - g \bar{h}_{i+1/2}^{k+1} S_{f\,i+1/2}^{\,k} \end{aligned} \tag{9}$$

where

$$\begin{aligned} q_{i+1/2} &= {}^*h_{i+1/2} u_{i+1/2}, \qquad \bar{h}_{i+1/2} = \frac{h_{i+1/2} + h_i}{2}, \\ \bar{q}_i &= \frac{q_{i+1/2} + q_{i-1/2}}{2}, \qquad S_f = \frac{\left(2h_i^k + b_i\right)}{b_i h_i^k} n^2 u_i^k \left|u_i^k\right|. \end{aligned} \tag{10}$$

The values of h and u with asterisks must be approximated, because their values are not known on the corresponding grid points. We calculate the values ${}^*h_{i+1/2}$ and ${}^*u_i$ using the upwind approximation of the first-order, as follows:

$${}^*h_{i+1/2} = \begin{cases} h_i & \text{if} \quad u_{i+1/2} \ge 0, \\ h_{i+1} & \text{if} \quad u_{i+1/2} < 0, \end{cases} \tag{11}$$

and

$${}^*u_i = \begin{cases} u_{i-1/2} & \text{if} \quad \bar{q}_i \ge 0, \\ u_{i+1/2} & \text{if} \quad \bar{q}_i < 0. \end{cases} \tag{12}$$

The next step is converting (9) into a semidiscrete scheme to obtain the rate of change of u with respect to t. Based on (8), we have the formulation:

$$\frac{d\bar{h}_{i+1/2}}{dt} = -\frac{\bar{q}_{i+1}^{\,k} - \bar{q}_i^{\,k}}{\Delta x} - \frac{q_{i+1/2}^k \left(b_{i+1} - b_i\right)}{b_{i+1/2} \Delta x}. \tag{13}$$

Substituting (13) into (9), we obtain:

$$\begin{aligned} \frac{du_{i+1/2}}{dt} &= \frac{1}{\bar{h}_{i+1/2}^{k+1}} \left(\frac{\bar{q}_{i+1}^{\,k}\, {}^*u_{i+1}^k - \bar{q}_i^{\,k}\, {}^*u_i^k}{\Delta x} \right) \\ &- \frac{1}{\bar{h}_{i+1/2}^{k+1}} \left(u_{i+1/2}^k \frac{\bar{q}_{i+1}^{\,k} - \bar{q}_i^{\,k}}{\Delta x} \right) - g \frac{h_{i+1}^{k+1} - h_i^{k+1}}{\Delta x} \\ &- g \frac{z_{i+1} - z_i}{\Delta x} - g S_{f\,i+1/2}^{\,k}. \end{aligned} \tag{14}$$

Hence, our mass conservative and momentum balance equations (6) and (7) become semidiscrete schemes (8) and (14).

To discretize (8) and (14) we can apply a discrete time integration using a standard solver of ordinary differential equations, such as, the first-order explicit Euler method. Therefore, the fully discrete schemes of our staggered-grid finite volume method are:

$$\begin{aligned} h_i^{k+1} &= h_i^k - \frac{\Delta t}{\Delta x} \left({}^*h_{i+1/2}^k u_{i+1/2}^k - {}^*h_{i-1/2}^k u_{i-1/2}^k \right) \\ &- \frac{\Delta t}{\Delta x} h_i^k\, {}^*u_i^k \frac{b_{i+1/2} - b_{i-1/2}}{b_i} \end{aligned} \tag{15}$$

and

$$\begin{aligned} u_{i+1/2}^{k+1} &= u_{i+1/2}^k - \frac{\Delta t}{\bar{h}_{i+1/2}^{k+1}} \left(\bar{q}_{i+1}^{\,k}\, {}^*u_{i+1}^k - \bar{q}_i^{\,k}\, {}^*u_i^k \right) \\ &+ \frac{\Delta t}{\bar{h}_{i+1/2}^{k+1}} u_{i+1/2}^k \left(\bar{q}_{i+1}^{\,k} - \bar{q}_i^{\,k} \right) \\ &- g \frac{\Delta t}{\Delta x} \left[\left(h_{i+1}^{k+1} - h_i^{k+1} \right) + \left(z_{i+1} - z_i \right) \right] + \Delta t S_{f\,i+1/2}^{\,k}. \end{aligned} \tag{16}$$

With these formulations, we have extended the work of Mungkasi *et al.* [8] as well as Stelling and Duinmeijer [10]. The strategy of involving the friction term due to Manning has been shown in the above derivations.

Up to here, we have achieved the first goal of this paper. Note that our first goal is to develop a numerical scheme (a finite volume method on staggered grids) to approximate the solutions to the shallow water equations involving source terms due to bottom topography, channel width, and Manning friction. The numerical schemes (15) and (16) are our proposed staggered method for solving the system of (6) and (7).

III. Results and Discussion

In this section, we conduct five numerical tests to achieve our second goal of this paper. That is, we want to analyze the influences of the friction factor with respect to water flows in the considered Saint-Venant model. The problems for the tests in this paper are taken from the paper of Mungkasi *et al.* [8].

For the discussion in this section, we define two additional variables. The first is the stage $w(x,t)=h(x,t)+z(x,t)$, that is, the vertical position of water surface measured from the horizontal x-axis reference. The second is the discharge $q(x,t)=h(x,t)u(x,t)$ which is actually the momentum in our one-dimensional problems when the channel has a constant width. Here,

$$Q(x,t)=b(x)q(x,t)$$

All measured quantities are assumed to have MKS units in the SI system. With this assumption, we omit the writing of units in all values of variables. In addition, the gravitational acceleration is $g=9.81$.

A. Case for constant topography and constant width

In this case, we take a dam break having width $b(x)=1$ and topography $z(x)=0$, as studied by Stoker [20]. The numerical schemes (15) and (16) are executed on the spatial domain $-100\le x\le 100$, and the simulation time is $0\le t\le 5$. We make partition to the spatial domain into 6400 cells in which 3200 of them are used to calculate the velocity $u(x,t)$ of water and the remaining are used to calculate the depth $h(x,t)$ of water. Here, $\Delta x=0.25$ is the defined cell width and $\Delta t=0.01\Delta x$ is the fixed time step. The depth has the initial condition:

$$h(x,0)=\begin{cases}10 & \text{if} \quad x\le 0,\\ 1 & \text{if} \quad x>0,\end{cases} \tag{17}$$

and $u(x,0)=0$ is the velocity initially. The left and the right boundary are:

$$u(-100,t)=u(100,t)=0,$$

and

$$h(-100,t)=10,\quad h(100,t)=1.$$

Results of this numerical simulation are shown in Fig. 3 for time $t=5$. We investigate the friction effects to the flow when the Manning coefficients are $n=0.00, 0.02, 0.04, 0.06$, respectively. We observe that the motion of water becomes slower when friction factor is greater. Slow motion of water has consequences in the increase of depth. This means that the greater the friction factor leads to the slower the water flow and the greater the depth.

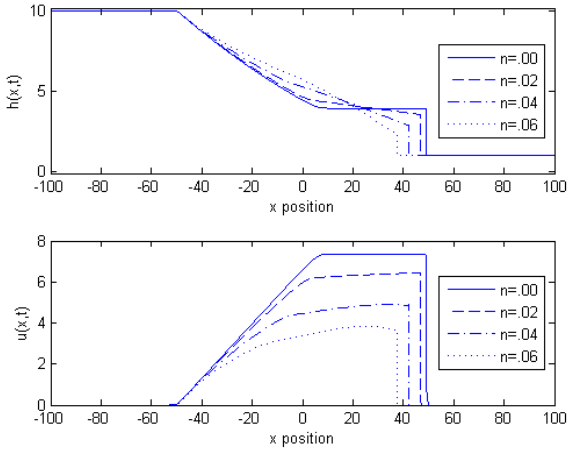

Fig. 3. Results of simulation for the dam break at t = 5 using 6400 cells.

B. Case for constant topography and irregular width

In this second test, the numerical method is applied to simulate flow generated by a radial dam which collapses instantaneously on a horizontal bottom topography. In this case, the channel width is $b(x)=2\pi x$ and the bottom topography is $z(x)=0$. The numerical schemes (15) and (16) are implemented on the spatial domain $[0, 100]$ and a numerical solution is computed for time $t=3$. We discretize the spatial domain into 400 cells (200 cells for the flow velocity and 200 cells for depth) with $\Delta x=0.25$ is the cell width. The time step is taken as $\Delta t=0.25\Delta x$. Before the vertical dam is removed, the depth has the initial condition:

$$h(x,0)=\begin{cases}10 & \text{if} \quad x\le 50,\\ 1 & \text{if} \quad x>50,\end{cases} \tag{18}$$

and $u(x,0)=0$ is the initial velocity. At the boundary, we have:

$$u(0,t)=u(100,t)=0,$$

and

$$h(0,t)=10,\quad h(100,t)=1.$$

Results of this numerical simulations are shown in Fig. 4 for time $t=3$. We vary the Manning friction coefficients to be $n=0.00, 0.08, 0.12, 0.16$. Similar results to the those of the first test are obtained. Water motion becomes slower when the friction factor is larger. Slow motion of water has increased the depth. This means that the greater the friction factor results in the slower the water flow and the greater the depth.

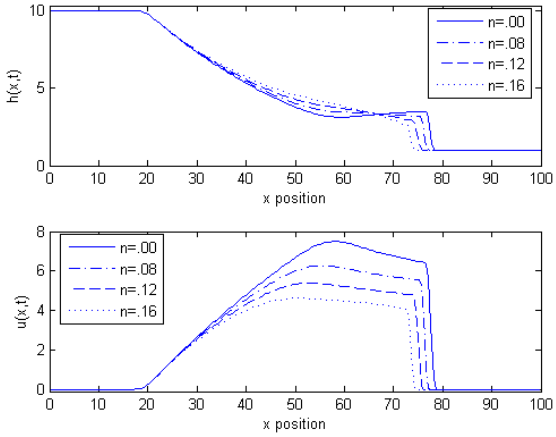

Fig. 4. Results of simulation for the radial dam break problem at t = 3 using 400 cells.

C. Case for irregular topography and constant width

In this third test, we have a parabolic obstacle on the topography. Let us take the steady state case of water flowswith constant width $b(x)=1$. Due to the obstacle, we have irregular bottom topography. The bottom topography is assumed to be defined by:

$$z(x)=\begin{cases}0.2-0.05(x-10)^2 & \text{if} \quad 8\le x\le 12,\\ 0 & \text{if} \quad \text{otherwise.}\end{cases} \tag{19}$$

The numerical schemes (15) and (16) are applied on the spatial domain [0, 25]. The number of the spatial cells is 800 in which a half of them are used to to calculate the velocity $u(x,t)$ and the others are used to calculate the depth $h(x,t)$.

The width of each cell is $\Delta x = 0.03125$ and the end time of numerical simulation is $t = 100$. The velocity is assumed to be $u(x,0) = 2.21$; and $w(x,0) = 2$ is the stage initially. The depth in downstream is $h(25,t) = 2$ and for the discharge in upstream is $q(0,t) = 4.42$. We take

$$\Delta t = 0.25\Delta x / \left(4.42/2 + \sqrt{g h_{\max}}\right)$$

as the time step, where $h_{\max} = 2$.

Results of this numerical simulation are shown in Fig. 5 respectively for the values of Manning coefficients $n = 0.00, 0.02, 0.04$. We observe that the velocity increases when water approaches the peak of the obstacle and decreases when water has passed the peak of the obstacle. Our inference is the same as in the two previous tests. That is, the water motion becomes slower when friction factor is involved in modeling. Slow motion of water has consequences to the increase of depth. The greater the friction factor leads to the slower the water flow and the greater the depth.

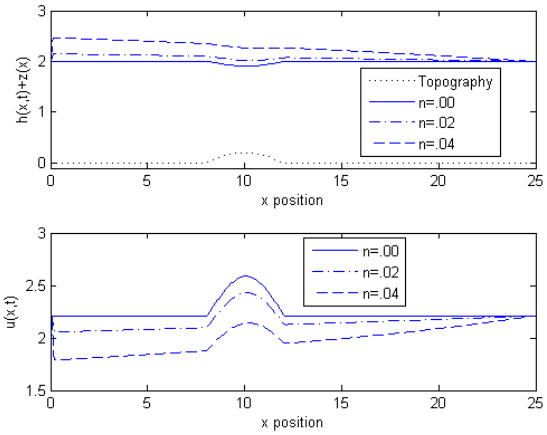

Fig. 5. Results of simulation for the steady flow over a parabolic obstacle at t = 100.

D. Case for irregular topography and irregular width

In this fourth test, we take the steady state of "a lake at rest" with irregular channel width and irregular bottom topography. The numerical schemes (15) and (16) are implemented on the spatial domain $0 \le x \le 1500$. The number of cells is 800 in which 400 cells are used to calculate the depth and the remaining are used to calculate the flow velocity. We take the velocity $u(x,0) = 0$ and the stage $w(x,0) = 12$ as the initial conditions. At the boundary we have:

$$u(0,t) = u(1500,t) = 0$$

and

$$w(0,t) = w(1500,t) = 12.$$

Here,

$$b(x) = 2\left\{1 + \exp\left[-\left(\frac{x-1000}{250}\right)^2\right]\right\} \qquad (20)$$

is the channel width. The channel profile viewed from the top is shown in Fig. 6, which is given in between the curves of $b(x)/2$ and $-b(x)/2$. Table 1 provides the bottom topography function, and together with the initial stage, it is plotted in Fig. 7.

Results of this simulation is shown in Fig. 8 for the Manning coefficients $n = 0.00, 0.02, 0.04$. We observe that our proposed numerical method is able to simulate the steady state problem of "a lake at rest" involving irregular bottom topography, irregular channel width, and friction. For time $t > 0$, where in Fig. 8 for $t = 10$, the water surface is always at $w(x,t) = 12$ and the velocity is at the order of 10^{-14}, which means that water is essentially at rest. Even though we use different values of Manning coefficients, our proposed numerical method is still able to solve this test problem.

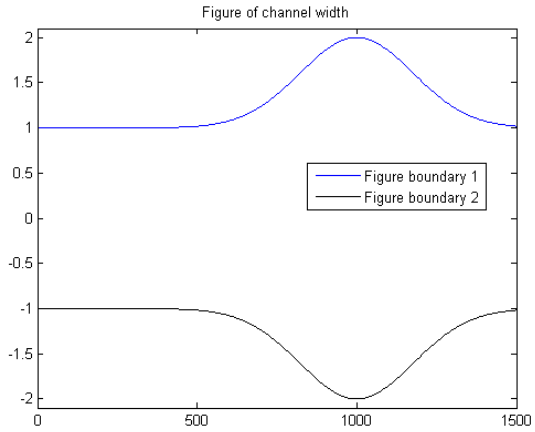

Fig. 6. The view from the top in the steady state of "a lake at rest."

TABLE I
TOPOGRAPHY FUNCTIONS OF THE CHANNEL BASED ON THE DATA AS IN THE WORK OF MUNGKASI *ET AL.* [8] TAKEN FROM GOUTAL AND MAUREL [21].

Interval	Topography function
$0 \le x < 50$	0
$50 \le x < 150$	$.05x - 2.5$
$150 \le x < 250$	5
$250 \le x < 300$	$-.04x + 15$
$300 \le x < 350$	$-.04x - 9$
$350 \le x < 400$	5
$400 \le x < 425$	$.1x - 35$
$425 \le x < 435$	$.05x - 13.75$
$435 \le x < 450$	$.0667x - 21$
$450 \le x < 475$	9
$475 \le x < 500$	$.004x + 7.1$
$500 \le x < 505$	$-.02x + 19.1$
$505 \le x < 530$	9
$530 \le x < 550$	$-.15x + 88.5$
$550 \le x < 565$	$-.0333x + 24.33$
$565 \le x < 575$	5.5
$575 \le x < 600$	$-.02x + 17$
$600 \le x < 700$	$.02 + 17$
$700 \le x < 750$	3
$750 \le x < 800$	$-.014x + 13.5$
$800 \le x < 820$	$-.015x + 14.3$
$820 \le x < 900$	$-.01x + 10.2$
$900 \le x < 950$	$-.016x + 15.6$
$950 \le x < 1000$	$-.008x + 8$
$1000 \le x \le 1500$	0

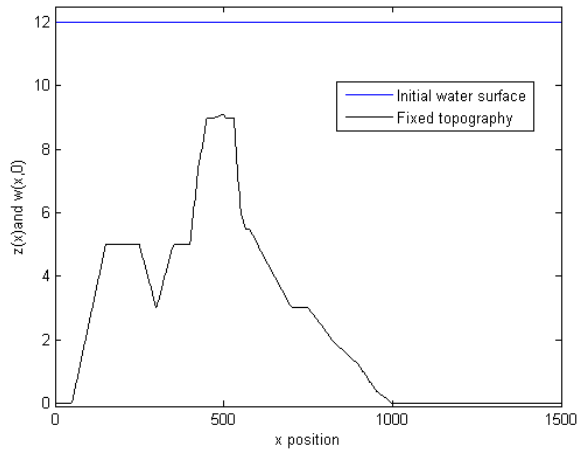

Fig. 7. Initial stage (water surface) and topography of "a lake at rest."

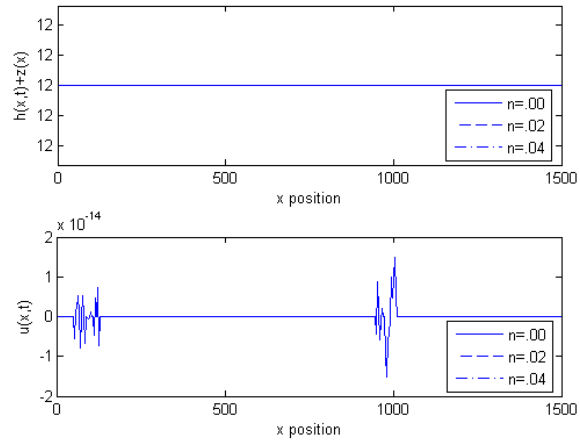

Fig. 8. Results for the steady state of "a lake at rest" at $t = 10$.

E. Simulation of irregular topography and irregular width

Here, we simulate an unsteady state case due to the collapse of a dam involving irregular channel width and irregular bottom topography. The numerical schemes in (15) and (16) are implemented on spatial domain [0, 2000]. We make a partition of this spatial domain to 1600 cells, so $\Delta x = 1.25$ is our cell width. In addition,

$$\Delta t = 0.25\Delta x / \left(4.42/2 + \sqrt{g h_{\max}}\right)$$

is our time step, where $h_{\max} = 2$. We simulate this problem until time $t = 90$. The bottom topography in this case is:

$$z(x) = \max\left\{0,\ \exp\left(-\left(\frac{x-1500}{100}\right)^2\right)\right\}. \qquad (21)$$

Here, the channel width is the same as in the previous test, that is, (20); and the channel width is shown in Fig. 6. The stage is initially given by:

$$w(x,0) = \begin{cases} 10 & \text{if} \quad x \le 1000, \\ 5 & \text{if} \quad x > 1000, \end{cases} \qquad (22)$$

and $u(x,0) = 0$ is given as the initial velocity. The conditions at the right boundary are $w(2000,t) = 5$ and $u(2000,t) = 0$. The conditions at the left boundary are $w(0,t) = 10$ and $u(0,t) = 0$.

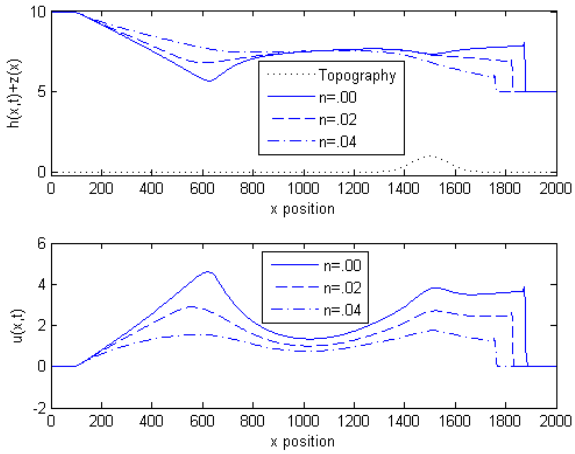

Fig. 9. Results of simulation for the unsteady state case of irregular topography and irregular width at $t = 90$.

Fig. 9 shows our numerical results for the variations of the Manning coefficients $n = 0.00, 0.02, 0.04$. We observe once again that water motion becomes slower when friction is involved in the problem.

IV. Conclusions

We have achieved our two goals in this paper. First, we have provided a numerical method for solving the shallow water equations in one dimension involving irregular bottom topography, irregular channel width, and friction. Second, using our proposed numerical method we have investigated some effects of friction to water flows along channels having irregular bottom topography, irregular channel width, and friction.

Our remarks are as follows. Our numerical method is able to solve problems of steady state and unsteady one, with horizontal topography and irregular one, with constant channel width and irregular one, without friction and with friction, as well as of combination of these all. In addition, larger friction factor leads to slower water motion, and consequently due to the momentum balance, larger friction factor also leads to greater depth when water is in motion.

This research is limited to one-dimensional problems with the friction due to Manning. Future research could be directed to work on higher dimensional problems and/or other friction formulations.

References

[1] A. J. C. B. de Saint-Venant, "Théorie du mouvement non permanent des eaux, avec application aux crues des rivières et à l'introduction des marées dans leur lit," *Comptes Rendus des Séances l'Académie des Sci.*, vol. 73, pp. 147–154, 237–240, 1871.

[2] J. A. Cunge, F. M. Holly Jr, and A. Verwey, *Practical Aspects of Computational River Hydraulics*. Boston: Pitman Advanced Publishing Program, 1980.

[3] K. Ostad-Ali-Askari, M. Shayannejad, S. Eslamian, and B. Navabpour, "Comparison of solutions of Saint-Venant equations by characteristics and finite difference methods for unsteady flow analysis in open channel," *Int. J. Hydrol. Sci. Technol.*, vol. 8, no. 3, pp. 229–243, 2018.

[4] G. Natasha, Suharjito, and V. Noviantri, "Saint-Venant model analysis of trapezoidal open channel water flow using finite difference method," *Procedia Comput. Sci.*, vol. 157, pp. 6–15, 2019.

[5] J. Balbás and S. Karni, "A central scheme for shallow water flows along channels with irregular geometry," *ESAIM Math. Model. Numer. Anal.*, vol. 38, pp. 821–852, 2004.
[6] W. Lai and A. A. Khan, "Numerical solution of the Saint-Venant equations by an efficient hybrid finite-volume/finite-difference method," *J. Hydrodyn.*, vol. 30, no. 2, pp. 189–202, 2018.
[7] V. Michel-Dansac, C. Berthon, S. Clain, and F. Foucher, "A well-balanced scheme for the shallow-water equations with topography or Manning friction," *J. Comput. Phys.*, vol. 335, pp. 115–154, 2017.
[8] S. Mungkasi, I. Magdalena, S. R. Pudjaprasetya, L. H. Wiryanto, and S. G. Roberts, "A staggered method for the shallow water equations involving varying channel width and topography," *Int. J. Multiscale Comput. Eng.*, vol. 16, no. 3, pp. 231–244, 2018.
[9] X. Xia and Q. Liang, "A new efficient implicit scheme for discretising the stiff friction terms in the shallow water equations," *Adv. Water Resour.*, vol. 117, pp. 87–97, 2018.
[10] G. S. Stelling and S. P. A. Duinmeijer, "A staggered conservative scheme for every Froude number in rapidly varied shallow water flows," *Int. J. Numer. Methods Fluids*, vol. 43, no. 12, pp. 1329–1354, 2003.
[11] R. J. LeVeque, *Numerical Methods for Conservation Laws*. Basel: Birkhäuser, 1992.
[12] C. Lu, L. Xie, and H. Yang, "The simple finite volume Lax-Wendroff weighted essentially nonoscillatory schemes for shallow water equations with bottom topography," *Math. Probl. Eng.*, vol. 2018, art. 2652367, 2018.
[13] A. Kurganov, "Finite-volume schemes for shallow-water equations," *Acta Numer.*, vol. 27, pp. 289–351, 2018.
[14] A. Kurganov, S. Noelle, and G. Petrova, "Semidiscrete central-upwind schemes for hyperbolic conservation laws and Hamilton–Jacobi equations," *SIAM J. Sci. Comput.*, vol. 23, no. 3, pp. 703–740, 2001.
[15] S. Mungkasi, "A study of well-balanced finite volume methods and refinement indicators for the shallow water equations," *Bull. Aust. Math. Soc.*, vol. 88, no. 2, pp. 351–352, 2013.
[16] S. Mungkasi, "Adaptive finite volume method for the shallow water equations on triangular grids," *Adv. Math. Phys.*, vol. 2016, art. 7528625, 2016.
[17] H. Ai, L. Yao, H. Zhao, and Y. Zhou, "Shallow-Water-Equation model for simulation of earthquake-induced water waves," *Math. Probl. Eng.*, vol. 2017, art. 3252498, 2017.
[18] B. A. Sulistyono and L. H. Wiryanto, "Investigation of flood routing by a dynamic wave model in trapezoidal channels," *AIP Conf. Proc.*, vol. 1867, art. 020020, 2017.
[19] B. A. Sulistyono and L. H. Wiryanto, "An analysis of the influence of variability rainfall on flow rate based on the watershed characteristics," *IOP Conf. Ser.: Earth Environ. Sci.*, vol. 124, art. 012001, 2018.
[20] J. Stoker, *Water Waves: The Mathematical Theory with Applications*. New York: Interscience Publishers, 1957.
[21] N. Goutal and F. Maurel, "Proceedings of the 2nd workshop on dam-break wave simulation," in *Technical Report HE-43/97/016/B, Electricité de France, Direction des études et recherches, Paris*, 1997.